Search for high-energy neutrinos from bright GRBs with ANTARES

A. Albert[1], M. André[2], M. Anghinolfi[3], G. Anton[4], M. Ardid[5], J.-J. Aubert[6], T. Avgitas[7], B. Baret[7], J. Barrios-Martí[8], S. Basa[9], V. Bertin[6], S. Biagi[10], R. Bormuth[11,12], S. Bourret[7], M.C. Bouwhuis[11], R. Bruijn[11,13], J. Brunner[6], J. Busto[6], A. Capone[14,15], L. Caramete[16], J. Carr[6], S. Celli[14,15,17], T. Chiarusi[18], M. Circella[19], J.A.B. Coelho[7], A. Coleiro[7], R. Coniglione[10], H. Costantini[6], P. Coyle[6], A. Creusot[7], A. Deschamps[20], G. De Bonis[14,15], C. Distefano[10], I. Di Palma[14,15], C. Donzaud[7,21], D. Dornic[6], D. Drouhin[1], T. Eberl[4], I. El Bojaddaini[22], D. Elsässer[23], A. Enzenhöfer[6], I. Felis[5], L.A. Fusco[18,24], S. Galatà[7], P. Gay[25,7], S. Geißelsöder[4], K. Geyer[4], V. Giordano[26], A. Gleixner[4], H. Glotin[27,28], T. Grégoire[7], R. Gracia Ruiz[7], K. Graf[4], S. Hallmann[4], H. van Haren[29], A.J. Heijboer[11], Y. Hello[20], J.J. Hernández-Rey[8], J. Hößl[4], J. Hofestädt[4], C. Hugon[3,4-UNI], G. Illuminati[14,15,8], C.W. James[4], M. de Jong[11,12], M. Jongen[11], M. Kadler[23], O. Kalekin[4], U. Katz[4], D. Kießling[4], A. Kouchner[7,28], M. Kreter[23], I. Kreykenbohm[31], V. Kulikovskiy[6,32], C. Lachaud[7], R. Lahmann[4], D. Lefèvre[33], E. Leonora[26,34], M. Lotze[8], S. Loucatos[35,7], M. Marcelin[9], A. Margiotta[18,24], A. Marinelli[36,37], J.A. Martínez-Mora[5], A. Mathieu[6], R. Mele[38,41], K. Melis[11,13], T. Michael[11], P. Migliozzi[38], A. Moussa[22], C. Mueller[23], E. Nezri[9], G.E. Păvălaş[16], C. Pellegrino[18,24], C. Perrina[14,15], P. Piattelli[10], V. Popa[16], T. Pradier[39], L. Quinn[6], C. Racca[1], G. Riccobene[10], K. Roensch[4], A. Sánchez-Losa[19], M. Saldaña[5], I. Salvadori[6], D. F. E. Samtleben[11,12], M. Sanguineti[3,30], P. Sapienza[10], J. Schnabel[4], F. Schüssler[35], T. Seitz[4], C. Sieger[4], M. Spurio[18,24], Th. Stolarczyk[35], M. Taiuti[3,30], Y. Tayalati[40], A. Trovato[10], M. Tselengidou[4], D. Turpin[6], C. Tönnis[8], B. Vallage[35,7], C. Vallée[6], V. Van Elewyck[7,28], D. Vivolo[38,41], A. Vizzoca[14,15], S. Wagner[4], J. Wilms[31], J.D. Zornoza[8], and J. Zúñiga[8]

[1]GRPHE - Université de Haute Alsace - Institut universitaire de technologie de Colmar, 34 rue du Grillenbreit BP 50568 - 68008 Colmar, France
[2]Technical University of Catalonia, Laboratory of Applied Bioacoustics, Rambla Exposició,08800 Vilanova i la Geltrú,Barcelona, Spain
[3]INFN - Sezione di Genova, Via Dodecaneso 33, 16146 Genova, Italy

[4]Friedrich-Alexander-Universität Erlangen-Nürnberg, Erlangen Centre for Astroparticle Physics, Erwin-Rommel-Str. 1, 91058 Erlangen, Germany
[5]Institut d'Investigació per a la Gestió Integrada de les Zones Costaneres (IGIC) - Universitat Politècnica de València. C/ Paranimf 1 , 46730 Gandia, Spain.
[6]Aix-Marseille Université, CNRS/IN2P3, CPPM UMR 7346, 13288 Marseille, France
[7]APC, Université Paris Diderot, CNRS/IN2P3, CEA/IRFU, Observatoire de Paris, Sorbonne Paris Cité, 75205 Paris, France
[8]IFIC - Instituto de Física Corpuscular (CSIC - Universitat de València) c/ Catedrático José Beltrán, 2 E-46980 Paterna, Valencia, Spain
[9]LAM - Laboratoire d'Astrophysique de Marseille, Pôle de l'Étoile Site de Château-Gombert, rue Frédéric Joliot-Curie 38, 13388 Marseille Cedex 13, France
[10]INFN - Laboratori Nazionali del Sud (LNS), Via S. Sofia 62, 95123 Catania, Italy
[11]Nikhef, Science Park, Amsterdam, The Netherlands
[12]Huygens-Kamerlingh Onnes Laboratorium, Universiteit Leiden, The Netherlands
[13]Universiteit van Amsterdam, Instituut voor Hoge-Energie Fysica, Science Park 105, 1098 XG Amsterdam, The Netherlands
[14]INFN -Sezione di Roma, P.le Aldo Moro 2, 00185 Roma, Italy
[15]Dipartimento di Fisica dell'Università La Sapienza, P.le Aldo Moro 2, 00185 Roma, Italy
[16]Institute for Space Science, RO-077125 Bucharest, Măgurele, Romania
[17]Gran Sasso Science Institute, Viale Francesco Crispi 7, 00167 L'Aquila, Italy
[18]INFN - Sezione di Bologna, Viale Berti-Pichat 6/2, 40127 Bologna, Italy
[19]INFN - Sezione di Bari, Via E. Orabona 4, 70126 Bari, Italy
[20]Géoazur, UCA, CNRS, IRD, Observatoire de la Côte d'Azur, Sophia Antipolis, France
[21]Univ. Paris-Sud , 91405 Orsay Cedex, France
[22]University Mohammed I, Laboratory of Physics of Matter and Radiations, B.P.717, Oujda 6000, Morocco
[23]Institut für Theoretische Physik und Astrophysik, Universität Würzburg, Emil-Fischer Str. 31, 97074 Würzburg, Germany
[24]Dipartimento di Fisica e Astronomia dell'Università, Viale Berti Pichat 6/2, 40127 Bologna, Italy
[25]Laboratoire de Physique Corpusculaire, Clermont Univertsité, Université Blaise Pascal, CNRS/IN2P3, BP 10448, F-63000 Clermont-Ferrand, France
[26]INFN - Sezione di Catania, Viale Andrea Doria 6, 95125 Catania, Italy
[27]LSIS, Aix Marseille Université CNRS ENSAM LSIS UMR 7296 13397 Marseille, France ; Université de Toulon CNRS LSIS UMR 7296 83957 La Garde, France
[28]Institut Universitaire de France, 75005 Paris, France
[29]Royal Netherlands Institute for Sea Research (NIOZ), Landsdiep 4,1797 SZ 't Horntje (Texel), The Netherlands
[30]Dipartimento di Fisica dell'Università, Via Dodecaneso 33, 16146 Genova, Italy
[31]Dr. Remeis-Sternwarte and ECAP, Universität Erlangen-Nürnberg, Sternwartstr. 7, 96049 Bamberg, Germany
[32]Moscow State University,Skobeltsyn Institute of Nuclear Physics,Leninskie gory, 119991 Moscow, Russia
[33]Mediterranean Institute of Oceanography (MIO), Aix-Marseille University, 13288, Marseille, Cedex 9, France; Université du Sud Toulon-Var, 83957, La Garde Cedex, France CNRS-INSU/IRD UM 110
[34]Dipartimento di Fisica ed Astronomia dell'Università, Viale Andrea Doria 6, 95125 Catania, Italy
[35]Direction des Sciences de la Matière - Institut de recherche sur les lois fondamentales de l'Univers - Service de Physique des Particules, CEA Saclay, 91191 Gif-sur-Yvette Cedex, France
[36]INFN - Sezione di Pisa, Largo B. Pontecorvo 3, 56127 Pisa, Italy
[37]Dipartimento di Fisica dell'Università, Largo B. Pontecorvo 3, 56127 Pisa, Italy
[38]INFN -Sezione di Napoli, Via Cintia 80126 Napoli, Italy
[39]Université de Strasbourg, CNRS, IPHC UMR 7178, F-67000 Strasbourg, France
[40]University Mohammed V in Rabat, Faculty of Sciences, 4 av. Ibn Battouta, B.P. 1014, R.P. 10000 Rabat, Morocco
[41]Dipartimento di Fisica dell'Università Federico II di Napoli, Via Cintia 80126, Napoli, Italy

Abstract

Gamma-ray bursts are thought to be sites of hadronic acceleration, thus neutrinos are expected from the decay of charged particles, produced in pγ interactions. The methods and results of a search for muon neutrinos in the data of the ANTARES neutrino telescope from four bright GRBs (GRB 080916C, GRB 110918A, GRB 130427A and GRB 130505A) observed between 2008 and 2013 are presented. Two scenarios of the fireball model have been investigated: the internal shock scenario, leading to the production of neutrinos with energies mainly above 100 TeV, and the photospheric scenario, characterised by a low-energy component in neutrino spectra due to the assumption of neutrino production closer to the central engine. Since no neutrino events have been detected in temporal and spatial coincidence with these bursts, upper limits at 90% C.L. on the expected neutrino fluxes are derived. The non-detection allows for directly constraining the bulk Lorentz factor of the jet Γ and the baryon loading f_p.

1 Introduction

The existence of hadronic acceleration mechanisms in Gamma-Ray Bursts (GRBs) would be unambiguously proven by the identification of high-energy neutrinos in temporal and spatial coincidence with the prompt emission of the burst. The detection of a single neutrino event would allow to identify this type of sources as a candidate for the Ultra-High-Energy Cosmic Ray (UHECR) production, whose origin is still under investigation (Blasi 2014). In order to test different scenarios, including those in which GRBs are able to reproduce the magnitude of the UHECR flux observed on Earth (see for instance Globus et al. 2015), a multi-messenger approach can be adopted. For this purpose, the search for a possible neutrino counterpart can be crucial. Indeed, neutrinos are ideal candidates in the search for distant astrophysical sources, as they are electrically neutral, stable and weakly interacting particles.

GRBs are transient sources, which release energies between 10^{51} and 10^{54} ergs in a few seconds (see Piran 2004, Mészáros 2006 and Zhang & Kumar 2015 for detailed reviews). Such extremely energetic events are probably related to the formation of a black hole, through the collapse of a massive star or the merging of a binary system (Piran 2004). The origin of GRB prompt emission is still under debate: the current theoretical understanding concerning the production of the γ-ray spectrum observed in the majority of GRBs is referred to as the standard fireball model (Piran 1999), which naturally produces a non-thermal spectrum. The generally accepted picture is the Internal Shock (IS) scenario (Rees & Meszaros 1994, Kobayashi et al. 1997 and Daigne & Mochkovitch 1998); nevertheless, the Photospheric (PH)

scenario has also been widely discussed in literature (Paczýnski 1986, Thompson 1994, Mészáros & Rees 2000 and Zhang & Kumar 2013). They both assume that internal shocks take place when a faster shell of plasma catches up with a slower one: such a mechanism dissipates a large fraction of the kinetic energy of the flow, provided that the internal engine is highly variable. A fraction of this energy is expected to be transferred to accelerated particles: acceleration takes place on a very short timescale at the shock front, leading particles to ultra-relativistic speeds. Accelerated electrons subsequently radiate a fraction of their energy through synchrotron and inverse Compton processes. This radiation field constitutes the target for photohadronic interactions: from the collision of accelerated protons with the dense radiation field of the jet, mesons are produced, which then decay, producing neutrinos and γ-rays.
The main channel goes through the production of the Δ^+ and its subsequent decay into pions, according to:

$$p + \gamma \rightarrow \Delta^+ \rightarrow \begin{cases} p + \pi^0 \\ n + \pi^+ \end{cases} \longrightarrow \begin{cases} \pi^0 \longrightarrow \gamma + \gamma \\ n \longrightarrow p + e^- + \overline{\nu}_e \\ \pi^+ \longrightarrow \mu^+ + \nu_\mu \\ \mu^+ \longrightarrow e^+ + \nu_e + \overline{\nu}_\mu \end{cases} \tag{1}$$

In this dense environment, also kaon contribution becomes relevant to γ-ray production, because of the energy losses before their decay, and to neutrino production, especially at high energies. The treatment of neutrino production models from the prompt emission of GRBs was first given by Waxman & Bahcall 1997 and in more detail by Guetta et al. 2004.
ANTARES (Ageron et al. 2011) is the largest undersea neutrino telescope on the Northern hemisphere, sensitive to neutrinos mainly with energies above hundreds of GeV. It is an array of photo-multiplier tubes (PMTs), anchored at a depth of 2475 m in the Mediterranean Sea, offshore Toulon (France). Neutrinos are detected through the Cherenkov radiation induced by ultra-relativistic particles created from a neutrino interaction. Track-like signatures are provided by muons, mainly produced by charged-current ν_μ interactions. Previous searches for neutrinos from GRBs with both the ANTARES (Adrián-Martínez et al. 2016, Adrián-Martínez et al. 2013a and Adrián-Martínez et al. 2013b) and IceCube (Aartsen et al. 2015, Aartsen et al. 2016) detectors did not measure any significant excess of neutrino events over the expected background and have placed limits on GRB parameters. Recent works (Baerwald, Bustamante, Murase & Winter 2015 and Bustamante, Murase & Winter 2016) suggest a GRB multi-zone production model for both neutrinos and cosmic rays, which significantly lowers the neutrino expected flux with respect to previous predictions, indicating that such a flux may have been overestimated in earlier works.

In this paper, a search for astrophysical neutrinos from bright GRBs with ANTARES data is presented. Bright sources represent promising targets, assuming that the neutrino flux scales with the γ-ray flux. In Sec. 2, four bright GRBs used in the search for neutrinos are introduced. Then, in Sec. 3, the internal shock and photospheric scenarios of the fireball model are briefly reviewed and the corresponding neutrino flux expectations are presented. Since the predicted signals are expected in different energy ranges, the analyses are performed using different data samples and specific features, as reported in Sec. 4, where the analysis methods are outlined. The results are discussed in Sec. 5. Because of the fact that no neutrino has been observed in coincidence with the GRBs, constraints on the parameter space of the models are given in Sec. 6: such constraints are derived for each GRB individually. Finally, the implications of such results on models for GRB neutrino production are examined in Sec. 7.

2 GRB selection

The search for point-like neutrino sources consists of the identification of an event excess over the expected background from a given position in the sky, where the source is located, as illustrated in Adrián-Martínez et al. 2014. In the case of GRBs, since the detected γ-ray emission is limited in time, also a temporal coincidence is required. In this way, it is possible to reduce the background contribution. The flux of atmospheric muons from above the detector comprises the largest part of the background, with a flux several orders of magnitude larger than any expected signal. The shielding effect of the Earth is exploited applying a geometrical cut on the reconstructed direction of the muon tracks. Selecting only upward going particles, the contamination by the atmospheric muons is largely reduced: since muons cannot cross the entire Earth, this cut rejects all atmospheric muons except for a small contamination due to mis-reconstructed events. In the study of transient sources, the requirement of temporal and directional coincidence allows to relax the cuts such that the dominant component is composed by mis-reconstructed atmospheric muons and atmospheric neutrinos, which represent an irreducible background for the cosmic signal. Therefore, an extended likelihood method is used to distinguish among signal and background events. For the search and simulation of neutrino fluxes, the brightest GRBs observable with ANTARES between 2008 and 2013 and the required γ-ray parameters are selected as described in Sec. 2.1. Both the theoretical IS and PH models have been used to predict neutrino fluxes.

2.1 GRB and γ-ray parameter selection

GRBs with high observed γ-ray fluence, namely bursts with $F_\gamma > 1\times10^{-4}\,\mathrm{erg\,cm^{-2}}$ (the average value of fluence ranges between 10^{-6} and $10^{-5}\,\mathrm{erg\,cm^{-2}}$), were selected. It is also required that the progenitors of such bursts have the redshift measured, in order to estimate their intrinsic luminosity, and that they were in the field of view of the ANTARES telescope at the trigger time, i.e. located below the horizon. Four bright GRBs fulfill these criteria: GRB 080916C, GRB 110918A, GRB 130427A and GRB 130505A. In order to compute neutrino spectra, some input parameters are needed. However, some of them, which mainly concern the mechanism through which the jet kinetic energy is converted into internal energy, cannot be directly inferred from measurements. As a consequence, default values are assigned to these inputs: the ratio f_p between internal energy in protons and electrons (also called baryonic loading) is fixed to $f_p = 10$; the fraction of internal energy in electrons ϵ_e and that in magnetic field ϵ_B are assumed equal because of energy equipartition, with $\epsilon_\mathrm{e} = \epsilon_\mathrm{B} = 0.1$; the average fraction of proton energy transferred to a pion is $\langle x_{p\to\pi}\rangle = 0.2$; and the Lorentz factor of the overall jet, more commonly denoted as bulk Lorentz factor, is $\Gamma = 316$. Also, when not explicitly mentioned, the minimum variability time is assumed to be $t_\mathrm{var} = 0.01$ s for long bursts: this parameter affects the evaluation of neutrino expectations, since it is directly related to the morphology of the internal source (Golkhou et al. 2015). Below the selection of the γ-ray parameters, as collected from the Gamma-ray Coordinate Network (GCN) Circular Archive[1] and reported in Tab. 1, is described and the search strategy applied burst per burst is presented.

GRB 080916C triggered γ-ray satellites at 00:12:46 UTC on September 16th, 2008, with a right ascension $\mathrm{RA} = 119.87°$ and declination $\mathrm{DEC} = -56.59°$. In a joint *Fermi* GBM and LAT analysis (Abdo et al. 2009) five time bins are defined, relying on the γ-ray spectral parameters. The relevant parameters for each bin in the burst are reported in Tab. 1. In particular, in bin B a 3 GeV photon was detected, followed by a 13.2 GeV photon in bin D: such high-energy emissions could be an indication of the hadronic origin of the radiation (Asano et al. 2011). Moreover, the redshift of the progenitor was identified at $z = 4.35$, while a minimum variability time scale of $t_\mathrm{var} = 0.23$ s was obtained from its light curve. Since neutrino production is directly linked to the GRB activity periods, our time dependent search is optimised in each of the five time bins defined by *Fermi* GBM and LAT analysis. The model expectations are therefore computed in each time bin and these contributions are summed up in order to obtain the expected signal from the burst.

[1] http://gcn.gsfc.nasa.gov/gcn3_archive.html

GRB 110918A started at 21:26:57 UTC on September 18th, 2011, located at $\mathrm{RA} = 32.58^\circ$ and $\mathrm{DEC} = -27.58^\circ$ with a redshift $z = 0.98$. Its local position in the ANTARES sky at the trigger time implied that neutrinos traveled up to the detector crossing the Earth quite horizontally, so that a negligible effect can be attributed to the Earth-absorption; this fact, together with the burst proximity in redshift, makes GRB 110918A a very promising candidate for a neutrino search with our detector. A time-dependent search is performed on this burst, based on data in three time bins given from the *Konus-Wind* satellite (Frederiks et al. 2013), as reported in Tab. 1. Frederiks et al. 2013 also estimate the minimum variability time $t_{\mathrm{var}} = 0.25$ s.

GRB 130427A enlight up the γ-ray sky on April 27th, 2013, at 07:47:07 UTC. From this burst two high-energy photons, of 95 GeV and 73 GeV, were detected by the *Fermi* LAT satellite (Ackermann et al. 2014). The source position was reconstructed at $\mathrm{RA} = 173.14^\circ$ and $\mathrm{DEC} = 27.71^\circ$ with a redshift $z = 0.34$. Its minimum variability time was measured to be $t_{\mathrm{var}} = 0.04$ s. The *Konus-Wind* Collaboration provided the time-dependent spectral parameters of the main emission episode.

GRB 130505A happened on May 13th, 2013, at 08:22:27 UTC and $\mathrm{RA} = 137.06^\circ$, $\mathrm{DEC} = 17.49^\circ$ at $z = 2.27$. Since the light curve of this burst is characterised by a main emission episode, a time average search was performed, relying on the spectral parameters released by *Konus-Wind* on the GCN. For this burst, the default value of t_{var} will be used in the following.

3 The Internal Shock and the Photospheric models

In GRB models, neutrinos are produced from the interaction between the accelerated protons and the jet radiation field. The predicted observable neutrino flux follows the primary spectrum; since both the internal shock and the photospheric models assume a differential energy spectrum for protons in the form of an unbroken power law with spectral index $s = -2$ (according to the Fermi first order acceleration mechanism in the test-particle regime), also the energy of neutrinos will be distributed according to a power law spectrum. Two breaks are expected to modify the simple power law behavior of neutrino energy distribution, both due to synchrotron cooling of charged particles. The former reflects the break in the photon spectrum due to energy losses of accelerated electrons: it directly affects the neutrino spectrum since neutrinos result from photo-production processes. The

Table 1: γ-ray parameters of each burst as detected from satellites (or, when not measured, assumed as default and marked with a *). Name of the burst; time bin in case of time-dependent analysis; duration T; fluence F_γ (measured in the energy range from 20 keV to 2 MeV for GRB 080916C and from 20 keV to 10 MeV for the others); low-energy spectral index α, high-energy spectral index β and peak energy E_γ of a Band spectrum (Band et al. 1993); redshift z; minimum variability time $t_{\rm var}$.

NAME	BIN	T (s)	F_γ (10^{-4} erg/cm^2)	α	β	E_γ (keV)	z	$t_{\rm var}$ (s)
GRB 080916C	A	3.6	0.15	-0.58	-2.63	440	4.35	0.23
"	B	4.1	0.21	-1.02	-2.21	1170	"	"
"	C	48.2	0.16	-1.02	-2.16	490	"	"
"	D	38.9	0.53	-0.92	-2.22	400	"	"
"	E	46.1	0.11	-1.05	-2.16	230	"	"
GRB 110918A	A	2.3	4.03	-1.95	-2.41	990	0.98	0.25
"	B	11.0	2.06	-1.00	-2.60	250	"	"
"	C	15.1	1.57	-1.20	-3.30	78	"	"
GRB 130427A	-	18.7	26.8	-0.96	-4.14	1028	0.34	0.04
GRB 130505A	-	7.0	3.13	-0.69	-2.03	631	2.27	0.01*

latter break is due to the synchrotron losses from secondary mesons. The main difference between the two scenarios is the radius at which acceleration takes place, since it affects the optical depth $\tau_{p\gamma}$ of pγ interaction (Zhang & Kumar 2013):

$$\tau_{p\gamma} = 0.8 \left(\frac{\mathrm{R}}{10^{14}\mathrm{cm}}\right)^{-1} \left(\frac{\Gamma}{10^{2.5}}\right)^{-2} \left(\frac{\mathrm{E}_\gamma}{1\mathrm{MeV}}\right)^{-1} \left(\frac{\mathrm{L_{iso}}}{10^{52}\mathrm{erg/s}}\right) \tag{2}$$

where Γ is the bulk Lorentz factor, R is the distance between the central engine and the neutrino production site which defines the fireball radius, $\mathrm{L_{iso}}$ is the isotropic γ-ray luminosity of the burst and E_γ is the energy at which the γ-ray spectrum has a break (of the order of 100 keV typically). In the IS scenario the radius of collision is (Piran 2004):

$$\mathrm{R_{IS}} = \frac{\mathrm{ct_{var}}}{1+\mathrm{z}}\Gamma^2 \sim 10^{13} \left(\frac{\mathrm{t_{var}}}{0.01\ \mathrm{s}}\right) \left(\frac{\Gamma}{10^{2.5}}\right)^2 \left(\frac{1+2.15}{1+\mathrm{z}}\right)\ \mathrm{cm} \tag{3}$$

where c is the light speed, t_{var} is the minimum variability time scale observed in the light curve of the burst and z is its redshift. The PH scenario predicts that particle acceleration occurs at a radius $\mathrm{R_{PH}}$ (Zhang & Kumar 2015) in such a way that γ-rays are unable to escape due to high optical depth of electron-photon scattering:

$$\mathrm{R_{PH}} = \frac{\mathrm{L_{iso}}\sigma_\mathrm{T}}{8\pi \mathrm{m_p c^3}}\Gamma^{-3} \sim 10^{11} \left(\frac{\mathrm{L_{iso}}}{10^{52}\mathrm{erg/s}}\right) \left(\frac{\Gamma}{10^{2.5}}\right)^{-3}\ \mathrm{cm} \tag{4}$$

where σ_T is the Thomson cross section of the interaction and m_p is the proton mass. Moreover, in the PH model, the dissipation of the jet energy takes place gradually and is distributed over a large fraction of the jet volume. For characteristic values of GRB parameters, Eq. 3 and Eq. 4 give $\mathrm{R_{PH}} < \mathrm{R_{IS}}$: $\tau_{p\gamma}$ in the PH model is enhanced by a factor $\mathrm{R_{IS}}/\mathrm{R_{PH}}$ compared to the IS model (see Eq. 2). Consequently, the neutrino production is more efficient in a dissipative photosphere than in standard internal shocks. Finally, as the neutrino energy breaks depend on the radius (Zhang & Kumar 2013), in such a way that increasing the collision radius moves neutrino energy breaks to higher energies, the resulting PH model produces neutrinos at lower energy $(100\ \mathrm{GeV} - 10\ \mathrm{TeV})$ than in the IS model $(100\ \mathrm{TeV} - 1\ \mathrm{EeV})$. Therefore, the neutrino signal predictions are very different between the two models, as shown in the following.

3.1 Neutrino flux expectations

In this section, the methods used for the computation of the expected neutrino fluxes from each GRB are presented: they rely on the event generator 'Neutrinos from Cosmic Accelerators'(NeuCosmA), described in Hümmer et al. 2010, for the

IS model case and on the analytical description from Zhang & Kumar 2013 in the PH model case.

3.1.1 Internal Shock Model Case

Detailed calculations of the GRB neutrino spectra in the IS context are performed, through the numerical code NeuCosmA. Based on SOPHIA (Mücke et al. 2000), it simulates the particle physics with a pre-defined proton and photon spectrum (here a GRB Band spectrum, Band et al. 1993) and takes into account the full pγ cross section, including not only the Δ^+ resonance but also higher mass resonances and kaon production. This yields an additional high-energy component in the ν_μ spectrum, typically at EeV energies. Moreover, it considers individual energy losses of secondary particles and neutrino oscillations during their propagation from the source to the Earth. The normalization of the neutrino spectrum is linearly scaled to the baryonic loading factor and to the per-burst γ-ray fluence. The algorithm produces the expected neutrino spectrum, assuming the measured values of the γ-ray parameters, as reported in Tab. 1 for each emission episode of the bursts. The resulting muon neutrino spectra are given as solid lines in the upper panel of Fig. 1.

3.1.2 Photospheric Model Case

To compute the PH neutrino spectra the general formalism developed by Zhang & Kumar 2013 was used, which adds a correction factor f to the normalization to take into account the fact that only a fraction of the accelerated protons will produce neutrinos via pγ interactions. These fluxes are shown as solid lines in the bottom panel of Fig. 1. Because the energy range of interest for this search is below 10 TeV, special features that could offer a better ANTARES sensitivity in the lower energy range have been used in this analysis: a sample of unfiltered data, a low-energy optimised reconstruction algorithm and a directional filter, as described in Sec. 4.1.

4 Methodology

Two different data samples are used in order to match the neutrino energy range expected from the two models, each with specific features concerning the track reconstruction algorithms, background evaluation and search time windows, as reported in Sec. 4.1. The same optimisation method is used for both models and is described in Sec. 4.2.

4.1 Data samples and specific analysis features

The ANTARES Data Acquisition (DAQ) system (Aguilar et al. 2007) is designed following the "all data to shore" concept: all photon signals are recorded above a threshold of 0.3 photo-electrons by the optical modules. They are then sent and buffered in the shore station where a filtering is performed. In some special cases, such as a GRB alert, the full unfiltered buffer can be saved on disk. The ANTARES detector receives the the GCN alert, which contains the position of the burst and its main features. In 90% of the cases the delay between the detection of a GRB by the satellite and the time of the alert message distributed is below 200 s (with a typical delay around 10 s). The GRB unfiltered data sample also includes unfiltered data buffered before the alert message reception. The overall size of the unfiltered data sample is about 2 minutes, so that data cover the majority of the burst duration (Bouwhuis 2005). To increase the sensitivity to low-energies, unfiltered data are used for the PH model, while filtered data are used for the IS one. The unfiltered data recorded are analysed with a dedicated algorithm, searching for space-time correlations restricted in a small search cone centered to the position of the considered GRB. A less strict filter condition with respect to the standard online triggers is applied. This algorithm yields more detected events in the target direction. A dedicated reconstruction algorithm (Visser 2015), optimised for energies below 1 TeV, is also applied to this specific data set. Through these new features and following the same search method presented in Sec. 4.2, but with a dedicated muon background estimation, the sensitivity improves by a factor of two at energies between 100 GeV and 1 TeV, where most of the neutrino flux is expected according to the PH model. The analysis performance is compatible with the one of the IS analysis at higher energies.

4.2 Analysis method

In order to simulate the per burst expected signal, the standard ANTARES Monte Carlo simulation chain has been used. It accurately describes the data taking conditions and the detector response during each GRB. The background for each burst is evaluated with data: upgoing atmospheric neutrinos are the main background component, with a smaller contribution coming from mis-reconstructed downgoing atmospheric muons. The number of background events μ_b expected in a defined angular and temporal window around the burst location is therefore assumed to be known *a priori*. The search time window in the IS analysis is chosen to be equal to each burst duration T (obtained as the sum of the time-bin durations) with a symmetric extension of 2 seconds. To be conservative, this extension is much larger than any effect due to the light propagation time from the satellite to our detector

and to uncertainties in the DAQ system. In the PH case, instead, the time window depends on the unfiltered data buffer duration. Since GRBs are transient sources, the angular window of the search can be enlarged with respect to that normally used in a steady source search (Adrián-Martínez et al. 2014): the search cone around the burst is fixed with an aperture equal to 10°. Given the short duration time window, this value still allows to have a rate of expected signal generally higher than the estimated background in the same search region, as will be shown later.
The analysis is optimised independently for each burst, as described in Adrián-Martínez et al. 2013b, through the computation of pseudo-experiments with $n_{\rm tot}$ total number of events, based on an extended maximum likelihood ratio test statistic Q (Barlow 1990):

$$Q = \max_{\mu'_s \in [0;n_{\rm tot}]} \Big(\sum_{i=1}^{n_{\rm tot}} \log \frac{\mu'_s S(\alpha_i) + \mu_b B(\alpha_i)}{\mu_b B(\alpha_i)} - \mu'_s \Big) \tag{5}$$

where α_i is the angular distance between the GRB position and the reconstructed muon direction, $S(\alpha_i)$ is the signal probability density function, obtained from Monte Carlo simulations, and $B(\alpha_i)$ is the background probability density function, assumed flat in the solid angle of the cone. In order to extract the distribution of Q as a function of the injected signals, more than 10^8 pseudo-experiments have been performed. Signal and background events are randomly extracted from their normalised distributions and the test statistic evaluated, returning the estimated signal μ'_s as the one maximising Q . The significance of a measurement is given by its p-value[2], that is the probability of getting values for Q at least as high as that observed if the background only hypothesis were true.
This procedure is repeated for different cut value of the track quality parameter (Adrián-Martínez et al. 2012): the finally selected value for this parameter is the one that maximises the probability to observe an excess with a p-value lower than the pre-defined threshold at a given statistical accuracy, assuming the expected signal flux from the model.

5 Results

Both analyses are optimised for the track quality cut yielding the maximum detection probability for a 3σ significance, with the background event rate μ_b evaluated as in Adrián-Martínez et al. 2013b. The results of the optimised IS analyses on the four bursts are summarised in Tab. 2. From these results, it is evident that for three

[2] A Gaussian two-sided convention is applied, with a 3σ background rejection corresponding to a p-value of $p_{3\sigma} = 2.7 \times 10^{-3}$.

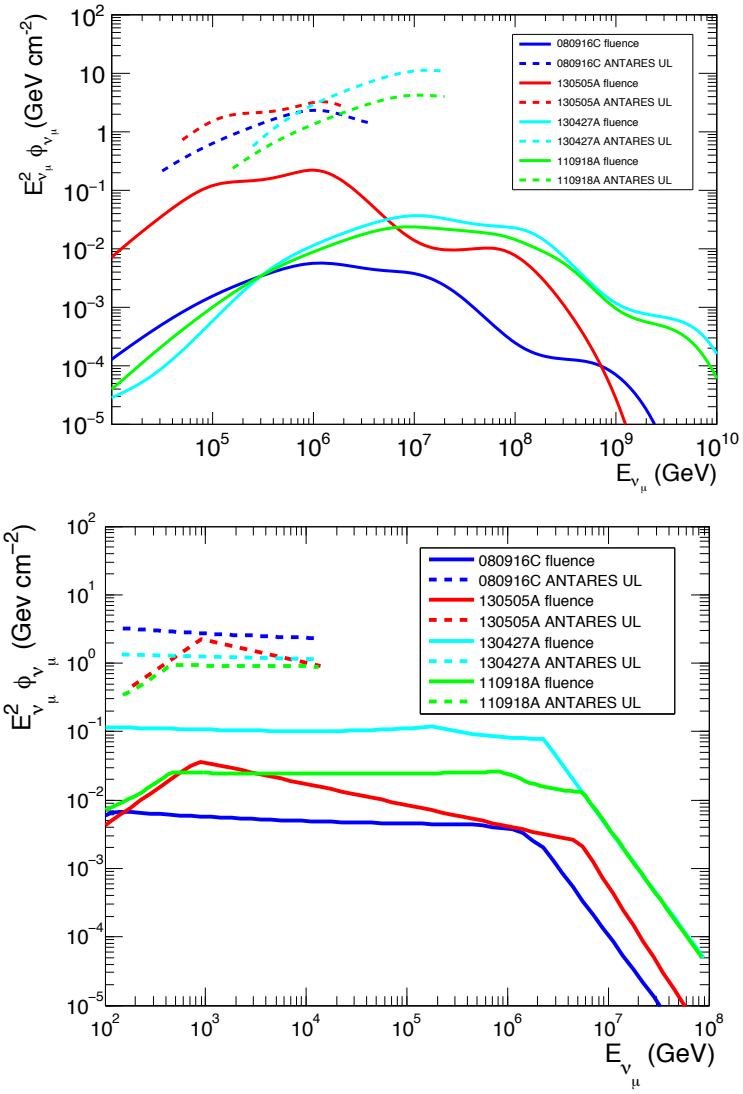

Figure 1: Solid lines: expected $\nu_\mu + \overline{\nu}_\mu$ fluences. Dashed lines: ANTARES 90% C.L. upper limits on the selected GRBs, in the energy band where 90% of the signal is expected to be detected by ANTARES. *Top:* IS model prediction (NeuCosmA). *Bottom:* PH model prediction.

Table 2: Optimised 3σ search for the four bursts, based on the IS model: columns report the optimised number of expected background and signal events, μ_b and μ_s respectively, and the probability to discover an excess (MDP) as predicted from the NeuCosmA model.

NAME	μ_b	μ_s	MDP
GRB 080916C	8.6×10^{-3}	1.8×10^{-3}	4.4×10^{-3}
GRB 110918A	7.2×10^{-3}	1.3×10^{-2}	1.5×10^{-2}
GRB 130427A	4.1×10^{-3}	7.5×10^{-3}	8.7×10^{-3}
GRB 130505A	2.4×10^{-3}	1.6×10^{-1}	1.5×10^{-1}

bursts (GRB 110918A, GRB 130427A and GRB 130505A) the estimated background μ_b is smaller than the expected signal μ_s.
After the analyses have been optimised for each burst, the different track quality cuts have been applied. In the PH case, the strategy described in Sec. 4.1 was applied on the unfiltered data files recorded in coincidence with GRB 130427A and GRB 130505A (since for GRB 080916C and GRB 110918A unfiltered data were not available). No events have been detected in spatial and temporal coincidence with any of these bursts in any of the time windows selected for the searches. 90% C.L. upper limits on the expected signal fluences are derived and reported in Fig. 1. Defining the differential neutrino fluence ϕ_ν, our limits are $E_\nu^2 \phi_\nu$ between about $[0.1 - 10]$ GeV/cm^2 for both models. Concerning the IS scenario, the closest upper limit to the expected flux is derived for GRB 130505A. This may also be related to the fact that it is the only burst of the sample for which the default value of minimum variability time scale has been used, because it was not directly measured. GRB 110918A and GRB 130427A give quite similar results: the better limit is on GRB 110918A, given the better effective area of the detector at the local position of this burst; the upper limit on GRB 080916C is on the other hand limited by its high redshift. For the PH scenario limits on the bursts for which unfiltered data were not available are obtained assuming no detection and using the optimised cuts of the IS analysis.

6 Constraints on GRB Models

The obtained 90% C.L. limits on the neutrino fluence allow the free parameters that significantly impact the neutrino flux to be constrained both in the framework of the IS and PH model. Since the measured γ-ray fluence F_γ, the bulk Lorentz factor Γ and the baryonic loading factor f_p mainly affect the neutrino yield from GRBs,

the use of bright GRBs is justified when assuming that such sources have broadly similar values of Γ and f_p. However, it is also essential to constrain the much larger sample of faint sources, since they could contribute to the diffuse neutrino flux with their cumulative effect. In Fig. 2 the 90% and 50% C.L exclusion limits are shown in the $\Gamma - f_p$ plane regarding the IS model predictions for GRB 130505A and the PH ones for GRB 130427A respectively, since these provide the strongest constraints. It is assumed that $1 \leq f_p \leq 200$ and $10 \leq \Gamma \leq 900$ and that the two parameters are not correlated.

6.1 Internal Shock Model Case

For the high-z burst GRB 080916C the derived constraints do not significantly challenge the internal shock model since values of Γ above 100 cannot be excluded. At low Lorentz factor regime $\Gamma < 100$, values of f_p in the range from 10 to about 30 are excluded but do not go beyond the default value of f_p. In the case of this GRB, the constraints are strongly limited because of the large distance to the source.

For the two bursts closest to the Earth GRB 130427A ($z = 0.34$) and GRB 110918A ($z = 0.98$) more stringent limits can be inferred. Low relativistic jets $\Gamma < 50$ are completely excluded and a baryonic loading factor is highly constrained to $10 < f_p < 20$ for $50 < \Gamma < 100$. For $100 < \Gamma < 200$ values of f_p greater than its benchmark value are excluded, while in the region with $\Gamma > 200$ f_p is barely constrained .

The most severe constraints are derived for GRB 130505A, starting to significantly challenge the IS scenario up to $\Gamma \sim 200$. This occurs mainly because GRB 130505A is much more energetic than GRB 130427A. In addition, because a short variability time scale was assumed (see Tab. 1), its internal shock radius ($R_{\rm IS} \propto t_{\rm var}$) is much smaller (which means that the pγ optical depth is enhanced) than that of GRB 110918A. However, contrary to GRB 110918A and GRB 130427A, this burst is much farther away ($z = 2.27$) which explains the poorest constraints on f_p at the very low Γ regime. Using a different value for the variability time scale, as $t_{\rm var} = 0.1$ s, the constraints are less restrictive and become of the same order of those from GRB 110918A and GRB 130427A.

6.2 Photospheric Model Case

The photospheric model is less sensitive to the bulk Lorentz factor variation mainly because of its Γ^{-3} radius dependency compared to the Γ^2 of the internal shock model. Thus the neutrino spectrum is mainly affected by the γ-ray fluence (and distance effects) and the baryonic loading factor of the sub-photospheric jet. For

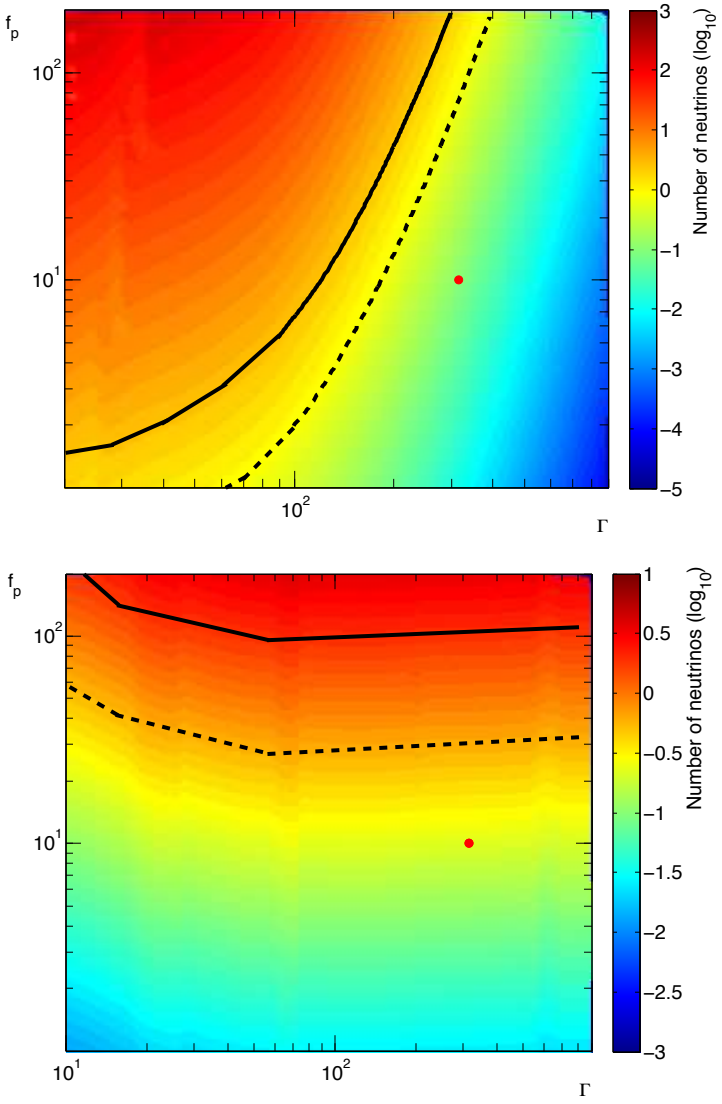

Figure 2: Number of expected neutrino events detectable with the ANTARES telescope (colored scale) computed as a function of Γ and f_p, in the context of the IS and PH models. The solid (dashed) black line corresponds to the exclusion limits at 90 (50)% C.L. The red dot shows the benchmark value $f_p = 10$ and $\Gamma = 316$. *Top:* IS constraints on GRB 130505A. *Bottom:* PH constraints on GRB 130427A.

these reasons less stringent constraints on f_p could be derived for GRB 130505A, GRB 080916C and GRB 110918A. For what concerns GRB 130427A, the closest and the most fluent burst, a high baryonic content (i.e. $f_p > 100$) in its jet has been ruled out.

7 Conclusions

A search for muon neutrinos in spatial and temporal coincidence with the prompt emission of four bright GRBs has been performed using ANTARES data. Events satisfying the optimised selection criteria have been considered in two independent analyses, with the purpose to test and constrain the parameters of both the internal shock and the photospheric scenarios of the fireball model. Concerning the internal shock model, the analysis has been optimised in order to give the highest model discovery potential for each burst, relying on the numerical model NeuCosmA. For the photospheric model the search strategy has been adapted using a dedicated data sample, able to enhance the sensitivity of the detector in the neutrino energy range between 100 GeV and 1 TeV, and optimised in the same way. No signal events have been detected in any of the searches, so that 90% C.L. upper limits on $E_\nu^2 \phi_\nu$ are derived. For the internal shock model, they are placed between 10^{-1} GeV/cm^2 and 10 GeV/cm^2 in the neutrino energy range going from 3×10^4 GeV to 2×10^7 GeV. For the photospheric model they stand in the same interval, but in the lower neutrino energy range from 1×10^2 GeV to 3×10^4 GeV. This search extends the ANTARES neutrino detection capability from GRBs into the low-energy regime; compared to what was shown in previous ANTARES searches for muon neutrinos in coincidence with 296 GRBs during four years of data (Adrián-Martínez et al. 2013b), it also confirms the sensitivity in the high-energy regime, i.e. above 100 TeV. Existing limits cannot rule out the theoretical models investigated here. It is worth recalling, however, that the expected neutrino fluence is normalised to the detected γ-ray emission: this allows to constrain the parameters affecting the GRB emission mechanism. In particular, limits on the bulk Lorentz factor and on the baryonic content of the GRB jet according to the IS/PH scenarios have been derived for each source. Assuming the internal shocks, for the closest burst the results suggest a low neutrino production efficiency because of the high Γ region still allowed. Such a picture is supported by the Lorentz factor estimation performed for the selected energetic bursts: $\Gamma = 870$ for GRB 080916C (Abdo et al. 2009), $\Gamma = 340 - 450$ for GRB 130427A (Hascoët et al. 2015 and Vurm et al. 2016) and $\Gamma = 340$ for GRB 110918A (Frederiks et al. 2013). This fact may work against the detection of high-energy neutrinos: the high neutrino production expected in the jet of the most fluent GRBs seems to be compensated by a high Lorentz factor

and possibly by a low baryonic loading. Models that assume that a low fraction of the GRB kinetic energy is transferred to protons (low f_p) if Γ is high are the most difficult to constrain using neutrino telescopes, as evident from Fig.2. The constraints do not exclude the hypothesis that, for a given jet energy, high values of Γ imply small values of f_p, as suggested by Sari & Piran 1995. This effect (low f_p if Γ is high) goes against the intuitive idea that the most energetic bursts (and generally the most fluent ones) are the best targets for individual neutrino detection. In the case of the photospheric scenario, on the other hand, less stringent constraints could be placed and most of the parameter space is still available.
The same constraints can in principle provide information on the allowed energy range and on the composition of primary particles. The connection between constraints in neutrinos and CR measurements indicates that a multi-messenger approach is a suitable strategy in the framework of testing the paradigm of GRBs as UHECR sources. Current neutrino telescopes have a small probability to detect neutrinos from GRBs, as shown in Tab. 2: further investigations of this scenario will be possible with the incoming generation of neutrino detectors, such as KM3NeT-ARCA (Adrián-Martínez et al. 2016) and IceCube-GEN2 (Aartsen et al. 2014).

Acknowledgements

The authors acknowledge the financial support of the funding agencies: Centre National de la Recherche Scientifique (CNRS), Commissariat à l'énergie atomique et aux énergies alternatives (CEA), Commission Européenne (FEDER fund and Marie Curie Program), Institut Universitaire de France (IUF), IdEx program and UnivEarthS Labex program at Sorbonne Paris Cité (ANR-10-LABX-0023 and ANR-11-IDEX-0005-02), Labex OCEVU (ANR-11-LABX-0060) and the A*MIDEX project (ANR-11-IDEX-0001-02), Région Île-de-France (DIM-ACAV), Région Alsace (contrat CPER), Région Provence-Alpes-Côte d'Azur, Département du Var and Ville de La Seyne-sur-Mer, France; Bundesministerium für Bildung und Forschung (BMBF), Germany; Istituto Nazionale di Fisica Nucleare (INFN), Italy; Stichting voor Fundamenteel Onderzoek der Materie (FOM), Nederlandse organisatie voor Wetenschappelijk Onderzoek (NWO), the Netherlands; Council of the President of the Russian Federation for young scientists and leading scientific schools supporting grants, Russia; National Authority for Scientific Research (ANCS), Romania; Ministerio de Economía y Competitividad (MINECO): Plan Estatal de Investigación (refs. FPA2015-65150-C3-1-P, -2-P and -3-P, (MINECO/FEDER)), Severo Ochoa Centre of Excellence and MultiDark Consolider (MINECO), and Prometeo and Grisolía programs (Generalitat Valenciana), Spain; Agence de l'Oriental and

CNRST, Morocco. We also acknowledge the technical support of Ifremer, AIM and Foselev Marine for the sea operation and the CC-IN2P3 for the computing facilities.

References

Aartsen M. G. et al. (IceCube Collaboration), 2016, Astrophys. J., 824 no.2, 115

Aartsen M. G. et al. (IceCube Collaboration), 2015, Astrophys. J., 805, L5

Aartsen M. G. et al. (IceCube-Gen2 Collaboration), 2014, E-print (arXiv:1412.5106v2)

Abdo A. et al. (Fermi LAT and Fermi GBM Collaborations), 2009, Science Mag, 323, 1688

Ackermann M. et al. (Fermi LAT Collaboration), 2014, Science Mag, 343, 6166,

Adrián-Martínez S. et al. (ANTARES Collaboration), 2012, Astrophys. J., 760, 53

Adrián-Martínez S. et al. (ANTARES Collaboration), 2013, J. Cosmology Astropart. Phys., 006

Adrián-Martínez S. et al. (ANTARES Collaboration), 2013, Astron. Astrophys., 559, A9

Adrián-Martínez S. et al. (ANTARES Collaboration), 2016, E-Print (arXiv:1608.08840)

Adrián-Martínez S. et al. (ANTARES Collaboration), 2014, J. Cosmology Astropart. Phys. 05, 0001

Adrián-Martínez S. et al. (KM3NeT Collaboration), 2016, J. Phys. G: Nucl. Part. Phys., 43, 084001

Ageron M. et al. (ANTARES Collaboration), 2011, Nucl. Instr. Meth., A, 656, 11-38

Aguilar J. A. et al. (ANTARES Collaboration), 2007, Nuclear Instr. and Methods in Phys. Res. A 570, 107-116

Asano K., Mészáros P., Murase K., Inoue S. & Terasawa T., 2011, Proceedings of 2011 Fermi Symposium

Bouwhuis M., 2005, Ph.D. thesis http://antares.in2p3.fr/Publications/thesis/2005/Mieke-Bouwhuis-phd.pdf

Baerwald P., Bustamante M., Murase K. and Winter W., 2015, Nat. Commun., 6

Band D. et al., 1993, Astrophys. J., 413, 281

Barlow R., 1990, Nucl. Instr. Meth., A, 297, 496

Blasi P., 2014, Comptes Rendus Physique 15, 2014, 329-338

Bustamante M., Murase K. and Winter W., 2016, E-print (arXiv:1606.02325)

Daigne F. & Mochkovitch R., 1998, MNRAS, 296, 275

Frederiks D. et al., 2013, Astrophys. J., 779, 151

Globus N., Allard D., Mochkovitch R. & Parizot E., MNRAS, 2015, 451, 1, 751-790

Golkhou V. Z., Butler N. R. & Littlejohns O. M., Astrophys. J., 811, 2

Guetta D., Hooper, D., Alvarez-Muniz J., Halzen F. and Reuveni E., 2004, Astropart.Phys. 20, 429-455

Hascoët R. et al., 2015, Astrophys. J., 813, 63

Hümmer S., Rüger M., Spanier F. and Winter W., 2010, Astrophys. J., 721, 630-652

Kobayashi S., Piran T. & Sari R., 1997, Astrophys. J., 490, 1

Mészáros P., 2006, Rept. Prog. Phys., 69, 2259-2322

Mészáros P. & Rees M. J. , 2000, Astrophys. J., 530, 292

Mücke A., Engel R., Rachen J. P., Protheroe R. J. and Stanev T., 2000, Computer Physics Communications, 124, 290-314

Paczýnski B., 1986, Astrophys. J. Lett., 308, L43

Piran T., 1999, Phys. Rept., 314, 575-667

Piran T., 2004, Rev. Mod. Phys., 76, 1143-1210

Rees M. J. and Meszaros P., 1994, Astrophys. J. Lett. 430, L93

Sari R. & Piran T., 1995, Astrophys. J. Lett., 455, L143

Thompson C., 1994, MNRAS, 270, 480

Visser E., 2015, Ph.D. thesis, Leiden University

Vurm I. et al., 2016, Astrophys. J. 831, 2, 175

Waxman E. and Bahcall J., 1997, Phys. Rev. Lett., 78, 2292

Zhang B. & Kumar P., 2013, Phys. Rev. Lett., 110, 121101

Zhang B. & Kumar P., 2015, Phys. Rep., 561, 1-109